# Combined Extraction and Functionalization of Low-Cost Nanoparticles from Municipal Solid Waste Fly Ash through PICVD

D.Farhanian, C.A.Dorval Dion, W.Raphael, G.De Crescenzo, J.R.Tavares*

Department of Chemical Engineering, Ecole Polytechnique de Montreal, C.P. 6079, Succ. Centre-Ville, Montreal, Quebec, Canada, H3C 3A7

## Abstract

While nanoparticles have been the focus of intensive research for several years as a result of their remarkable surface-driven properties, they remain, for the most part, stuck in the lab. This unfortunate fact can be explained by three main reasons: (1) most studies have not dealt with the scalability and cost issues related to the use of nanomaterials on an industrial scale; (2) a great deal of focus has been applied to "outlier" results that promise far more than can be delivered; and (3) very little attention has been given to surface engineering. We propose to curtail the significant cost issue by extracting low-cost, low-grade nanoparticles that are appropriate for several applications from a ubiquitous and abundant feed stock: fly ash from municipal solid waste (MSW) incineration. The novel technique we apply is capable of both extraction and functionalization of the nanoparticles present in this undervalued waste stream using photo-initiated chemical vapor deposition (PICVD). By setting functionalization conditions to favor hydrophilic surface properties, the treated ash can readily be dispersed in a polar solvent such as water: larger particulates then settle out of suspension, while the lighter nanoparticles remain in the supernatant and are ready for use. While it is true that this method yields low-grade nanoparticles (polydisperse and multi-composite), these can be used in a variety of applications where composition is less crucial, such as increasing the thermal conductivity of composites and nanofluids.

**Keywords:** PICVD, Nanoparticles, Functionalization, Surface functionalization, MSW fly ash

## Nomenclature

MSW Municipal Solid Waste

PICVD Photo-Initiated Chemical Vapor Deposition

PECVD Plasma Enhanced Chemical Vapor Deposition

TEM Transmission Electron Microscopy

EDS Energy-Dispersive X-ray Spectroscopy

FTIR Fourier Transform Infrared Spectroscopy

∗Corresponding author: jason.tavares@polymtl.ca

## 1. Introduction

Even if nanoparticles are omnipresent in research laboratories, the cost of these advanced materials remains a limiting factor to their widespread implementation. While the usage of expensive, pure and spherical nanoparticles made from exotic materials can be justified for some high-end applications like drug carriers and microelectronics, some more modest applications call for cheaper sources of nanoparticles [1, 2]. In the hope of finding cheaper alternatives, attention has recently been paid to unconventional sources of ultrafine powders, such as ash from the incineration of municipal solid waste (MSW), coal, cane or oil shale [1, 3-8]. Indeed, several studies focused on the type and level of nanoparticles present in the ash residues [1, 9-11]. Such interest is mainly justified because the accumulation of large quantities of ash is becoming a serious environmental problem [5, 12-16]. Both MSW and fly ash are considered as renewable resources due to their valuable materials content [3, 13, 15, 17, 18]. They also constitute an important debate due to their toxicity, causing important cardiopulmonary diseases at low concentrations [16, 18-20].

The interesting aspect of using fly ash is that it does not really have any value on the market, since it is currently disposed of in landfills or used in cements [5, 18]. However, valorization through use as a cement additive or filler is still in development in the case of MSW fly ash. Indeed, many jurisdictions do not allow its use because of its potential hazardous materials content. For jurisdictions where it is permitted for use as a supplementary cementitious material (SCM), additional long-term durability testing is underway [21-24]. Furthermore, it must be taken into account that if fly ash is affordable, it is far from being usable as is for many reasons: (1) the substances are not pure, (2) the chemical composition is variable (particularly if sourced from MSW) and (3) the particle size distribution is wide and variable. The use of fly ash also restrains the selection of materials available; indeed, it often contains minerals such as illite, kaolinite, chlorite, calcite, alumina and quartz; in other words, metals are present in oxidized form [6, 16, 18]. Indeed, the composition can vary according to the source of the ash, but typical compositions are silica (49-64 % wt), alumina (14-30 % wt), iron oxide (6-23 % wt) and CaO (1-7 % wt)

[1, 5, 6, 12, 13]. That means that the intended end-use must either encourage the use of such minerals and derivatives, or not be sensitive to the nature of the material at all. An example of the former would be any usage that is suited to silica ($SiO_2$), which can be used as an additive to cement [3, 4] or rubber matrices [13, 25] to improve their mechanical properties, or as an adsorbent and catalyst support due to its physical chemistry properties [11, 19]. On the other hand, MSW fly ash contains some valuable materials including As, Al, B, Ba, Cd, Cr, Cu, Hg, Mn, Mo, Ni, Pb, Sb, Se, Zn, in oxidized or ionic salt form [26, 27]. In case the composition is not a problem, these nanomaterials can be used in order to increase the overall thermal conductivity of the composites [28-30] and nanofluids [31-33]. For applications more sensitive to particle size distribution or chemical composition, the nanomaterials can be further treated before use, through size segregation [2, 32, 34] or chemical treatment [2, 29, 30, 35].

Recently, several studies focused on implementation of nanoparticles as filler in production of composite using in situ polymerization technique [29, 30]. However, there are some challenges in composite fabrication using nanoparticles: (1) introduction of good chemical bonds between polymer and nanofiller, and (2) homogeneous dispersion of nanofillers due to their agglomeration [29, 30]. These challenges can be resolved using chemically engineered (functionalized) nanoparticles [28-30].

These recent studies clearly demonstrate that nearly all raw nanomaterials need to be surface functionalized prior to incorporation into matrices. While a vast amount of energy has been spent on extraction of nanomaterials from ash, no one seem to have addressed functionalization. Our group is mainly concerned about the feasibility of combining extraction and functionalization with existing processes to generate nanoparticles. The process proposed to chemically transform the material is usually by sol-gel techniques, which seem hardly scalable due to significant use of acidic solutions and subsequent wastewater control [17, 18, 27]. Our group previously identified photo-initiated chemical vapor deposition (PICVD) as a potential affordable and scalable technology for the surface functionalization of nanoparticles [36]. This technique had been applied in our research group for the functionalization of copper (Cu) coupons using syngas and UVC lamps [37]. Subsequently, by considering the applications where composition is less crucial, such as nanofluids, our group investigated to see if such a surface treatment could be sufficient to recover ready-to-use nanoparticles from fly ash. This study proposes a novel method for the single-step extraction and functionalization of nanoparticles from a low-value raw source, municipal solid waste (MSW) incineration fly ash, using PICVD for functionalization.

## 2. Materials and Methods

MSW fly ash was provided by the Quebec City MSW incinerator. This waste residue is selected in order to verify the effectiveness of our process for what we consider to be the most difficult class of fly ash to treat, as it has the widest range of particle sizes and materials composition. Thus, it will demonstrate the range and versatility of our process. Ash powder was sieved using meshes with 300 µm, 150 µm, and 75 µm size. Then, 1 g of ash powder from the less than 75 µm fraction was used for the experiments. The PICVD technique was then applied for functionalization of particles in ash samples.

### 2.1. PICVD Experimental Apparatus

Figure 1. shows the schematic of the experimental apparatus. The PICVD unit consisted of: two 254 nm UVC mercury or germicidal lamps as an initiation source (Cole-Parmer) and a 45 cm long quartz reactor using standard 24/40 taper joints (Technical Glass Products). The UVC lamps had a main peak at a wavelength of 254 nm. Syngas (CO and $H_2$) was used as the functionalization precursor (CO: Pur T-44 and $H_2$: UHP T-30 - Air Liquide). Although, these reactants are not in the peak absorption of UVC lamps (254 nm), they can be activated at 254 nm and produce active compounds for the formation of functionalized polymeric films [37]. Argon gas (HPT - Air Liquide) was used to purge the reactor before experiments to remove oxygen. For some experiments, $H_2O_2$ (50% aqueous solution- Fischer Scientific) was added as a photoinitiator to accelerate reaction kinetics and enhance the polymerization rate [38], this was done using a syringe pump at a rate of 0.02 mL/min. Experiments were performed either under slight vacuum (-10 kPa) or at near atmospheric pressure (+10 kPa) regulated by a T-valve at the end of reactor. The irradiance of the UVC lamps was measured at 3.5 cm away from the lamp (in the same distance of reactor from the lamps) using an ILT1700 radiometer/photometer coupled with a SED240/QNDS2/W254 nm sensor (International Light Technologies). The average irradiance at this distance was $5.5 \times 10^{-4}$ $W/cm^2$.

**[Figure 1 about here.]**

### 2.2. Extraction and Functional Encapsulation of Nanoparticles from Ash powder

At first, 1 g of ash powder was loaded in a metal holder and inserted to the reactor. Oxygen molecules are strong electron scavengers; thus, their presence will result in termination of reactions. To avoid this, reactor was purged using argon gas for 5 minutes. Then, the mixture of CO: 390.1 mL/min and $H_2$: 48.7 mL/min was injected into the reactor ($H_2$/CO ratio of 12.5%) [38]. Experiments were performed either

while (1) UVC lamps were turned on, or (2) they were turned off (control experiments - syngas was flowing in the reactor). Duration of experiments was fixed to 1h. Temperature inside the reactor was monitored during experiments using an infrared temperature sensor. The measured temperature was 30 ± 7 $^{0}$C. Table 1. summarizes the details of all experiments. Treated ash powders were then dispersed in deionized water or acetone and the resulting samples were loaded in an ultrasonic bath for 2h in order to disperse the particles. The large particulates are then allowed to settle for 24 hours before the liquid supernatant was collected for analysis.

**[Table 1 about here.]**

### 2.3. Characterization and Analytical procedures

Field Emission Scanning Electron Microscopy (FESEM) (JEOL JSM7600F) were used to investigate the morphology of untreated ash powder. Using the Scanning Electron Microscopy (SEM) (JEOL 840A), three Energy Dispersive X-ray spectra were acquired in different regions to determine the elements present in the sample. Moreover, in order to have better understanding of the compostion of ash samples, elemental analysis had been performed using Inductively Coupled Plasma Optical Emission Spectroscopy (ICP-OES, Thermo Scientific iCAP 6500). To do so, about 0.5 g of ash powder was digested in 5 mL of hydrochloric acid and 2 mL of $HNO_3$ solution then heated for 150 min on a hot plate at 95 °C. Then the remaining solution was diluted with deionized water in 50 mL digi tubes and filtered using a 0.45 µm-pore PTFE filter and analyzed in ICP-OES. Two standard reference materials (Routine Quality Control Solution: RQC-1 and RQC-2, SCP Science) were used to verify the analytical quality of the measurements.

To assess which crystalline phases are present in the raw ash, untreated MSW ash powders were analysed by XRD (Philipps X'Pert system) using Cu Kα radiation. Scans were conducted from 20.01 to 89.99 ° at a rate of 0.02° 2Θ/min. X'Pert Highscore (Philipps) software was used to identify possible crystalline phases.

Dispersed solids remaining in the supernatant were analyzed using Transmission Electron Microscopy (TEM, model JEM 2100F-JEOL company) in combination with energy-dispersive X-ray spectroscopy (EDS). TEM was operated at 200 kV to acquire bright field images of samples. Morphology and elemental analyses for extracted nanoparticles were conducted using copper (Cu) and nickel (Ni) TEM grids coated with a lacey carbon film (D20040 Grids with formvar substrates mesh 400, metal Cu; D20045 Grids with formwar substrates mesh 400, metal Ni-SOQUELEC International). The grids were

first soaked in the liquid samples and then in the deionized water for few seconds in order to avoid salt contamination on the grids. Then, samples were dried at the room temperature $22 \pm 2.5\ ^{0}C$ and analyzed. All experimental conditions were repeated at least twice and analyzed using both types of TEM grids in all cases.

After sampling, the remaining supernatant was dried overnight at $55\ ^{0}C$ and analyzed by Diffuse Reflectance Fourier Transform Infrared Spectroscopy (DRIFTS, Thermo Scientific Nicolet 6700 ) to obtain chemical information about the coating and functional organic groups. OMNIC software was used to identify the corresponding peaks. Each sample was scanned 32 times with a resolution of 4.0 $cm^{-1}$. No addition of KBr was necessary for the analysis – samples were directly analyzed in the DRIFTS apparatus to obtain FTIR spectra of solid samples.

## 3. Result and Discussion

**Physical characterization:** Figure 2 shows FESEM micrographs, along with accompanying EDS spectra, of MSW ash powder before any experiments. This result showed that ash sample contains mainly the following elements : Si, Al, O, Ca, Na, Cl, K, P, Mg, S, Ti and Fe. The SEM micrographs serve to illustrate the wide size distribution of the untreated ash.

**[Figure 2 about here.]**

Table 2 shows the elemental concentration of untreated MSW ash powder. The rest of ash powder is carbon (C) and water ($H_2O$).

**[Table 2 about here.]**

XRD results of crystalline phase of MSW ash powder before any experiments can be found in Figure 3.

**[Figure 3 about here.]**

This result shows that MSW ash sample contains a large number of phases which makes the XRD analysis quite uncertain. The large number of peaks makes it possible for many reference patterns (phases) to show a high score of fit with the XRD measurement even if they are not necessarily present. By using the EDS results shown in the Figure 2, we can refine the search in the database to find reference patterns that match the measurement. Taking this into account, the samples contains $SiO_2$, $CaCO_3$ and NaCl and may contain one or more of these phases : $KFeO_2$, $KAlSi_3O_8$, $CaAl_2Si_2O_8$, $Al_2(PO_4)(OH)_3$ and

179 $(Na,Ca)Al(Si,Al)_3O_8$. It is possible and quite probable that other phases are present in this sample, but
180 were either not detected by XRD or were not identified by searching the database.

181 Figures 4 and 5 show, respectively, the TEM/EDS results of PICVD-untreated and treated ash samples.
182 Results for control experiment (#1, Table 1) in Figure 4 indicate that there are little or no metal
183 nanoparticles present, except Ca in oxidized form, demonstrating that there is limited potential to extract
184 useful nanoparticles without a functionalization treatment. The TEM micrograph also illustrates the
185 presence of salt (lower-contrast particulates). This by-product is contained in the ash samples, both
186 natively or as a result of the gas cleaning steps applied during the waste incineration process.

187 **[Figure 4 about here.]**

188

189 The TEM/EDS results of experiments #2 to #5 (Table 1) in Figure 5 demonstrate the presence of nano
190 size particles in the supernatant of treated ash samples. The nanoparticles found in these samples vary
191 based on the composition of the primary ash sample. Two types of grids had been used in order to
192 identify possible Cu and Ni nanoparticles in the samples. EDS analysis was performed on different
193 sections of the grids, confirming the presence of Si, Al, Zn, and Fe as dominant nanoparticles in all of the
194 samples, as well as Cu, Sn, Pb, and Mg.

195 **[Figure 5 about here.]**

196

197 Lower-contrast salt particulates were also visible for these experiments. These can be removed through
198 successive rinsing steps with water. These results show that extraction of nanoparticles either in the
199 presence or in the absence of $H_2O_2$ is possible. From treatment to treatment, the same type of
200 nanoparticles can be extracted. However, at this time, only qualitative study were performed, further
201 quantitative study is warranted.

202 Several nanofillers like copper oxide (CuO and $Cu_2O$) [29], iron oxide (FeO, $Fe_2O_3$ or $Fe_3O_4$) [39], zinc
203 oxide (ZnO) [40], $CaCO_3$ [28, 30], silica or silicon carbide [35, 41], and aluminum oxide ($Al_2O_3$) [42]
204 have been applied for in situ polymerization, as previously discussed. These nanoparticles can increase
205 electrical conductivity, photovoltaic properties, thermal conductivity and thermal stability of the
206 composite. Almost all of these compounds can be found in the MSW ash samples treated by our method.

207 While nanoparticles were found generally in agglomerated form, the treated agglomerates remain of
208 interest. Moreover, the facile extraction technique presents other advantages (1) it can more readilty be

implemented compared to other functionalization techniques [36], (2) it allows for the extraction of useful nanoparticles allowing clean and closed industrial scale production cycles and, (3) it nonetheless allows for stable dispersion of nano-sized particulates because of their functional coating.

As presented, our method allows for the extraction of nanoparticles with multiple components. Other works have focused on the selective extraction of specific materials either by targeted acidic attack or use of target flocculants [17, 18, 27]; through further work, these techniques could be combined with our method. Nonetheless, the low-grade particles we can extract may find applications in various fields.

In order to extend the range of applications, dispersion in other solvents has been briefly studied. To do so, treated ash samples were dispersed in a less polar solvent - acetone (polarity index of 5.1, compared to water at 9.0 [43]). TEM/EDS results (Figure 6) showed identical nanoparticles, which demonstrates that either polar (water) or semi-polar (acetone) solvents can be applied for extraction of nanoparticles.

**[Figure 6 about here.]**

Syngas (CO and $H_2$) is one of the common products of gasification processes. It can be used for hydrocarbon formation through the Fischer-Tropsch Synthesis (FTS) pathway. In our case, rather than target recombination of long hydrocarbon chains, we aim to deposit the radicals produced in the presence of UVC lamps onto substrates – the proposed reaction pathway has been discussed in our previous work [37].

**Chemical Characterization:**In order to verify this deposition, DRIFTS analysis was performed to study the organic coating and identify functional groups. Figure 7 and 8 shows the DRIFTS spectra taken from experiments #1 to # 6 . Table 3 represents the likely assignments of the identified peaks in the DRIFTS spectra.

**[Figure 7 about here]**

**[Figure 8 about here]**

Spectra for control experiment ( Experiment #1) shows only –OH functionality due to the adsorption of humidity in 3600-3100 $cm^{-1}$. In the case of experiments #2 to #5, which were dispersed in water, clearly, these spectra shows almost similar features and organic coating functionalities. However, the intensity of functional groups is different. The very broad peaks in the 3600-3100 $cm^{-1}$ range strongly indicate presence of hydroxyl groups (-OH stretch from both covalently bonded hydroxyl groups and absorbed

moisture). This peak overlaps the C-H stretch around 2930 $cm^{-1}$. There is also a C-O single bond band near 1100-1300 $cm^{-1}$ specifically in the 1000-1070 $cm^{-1}$ and 1240 $cm^{-1}$ ranges, which demonstrate formation of primary alcoholic functional groups as well as phenol groups respectively. In the case of experiment #3, the presence of peaks around 1240 $cm^{-1}$ shows the formation of higher amounts of phenol groups. This means a more aromatic structure was formed in this case compared to the other experimental conditions. Amounts of hydroxyl groups are almost identical in the case of experiments #3, #4, and #5 and they are greater in these experimental conditions compared to experiment #2 and #6. In experiments #3 and #5, $H_2O_2$ was used as a photoinitiator, as it can form hydroxyl groups under UVC (254 nm) irradiation due to photolysis. Hydroxyl groups formed due to photolysis of $H_2O_2$ molecules can act as reactive compounds and participate in chain reactions either with CO or $H_2$ molecules or their radicals [22, 38, 44, 45]. Subsequently, more hydroxyl functionality produces in the presence of $H_2O_2$ which leads to a more hydrophilic coating (Equations (1) to (6)).

$$H_2O_2 + hv\ (254\ nm) \rightarrow 2\ OH^{\bullet} \quad (1)$$

$$H_2O_2 + OH^{\bullet} \rightarrow H_2O + O_2^{-} + H^{+} \quad (2)$$

$$H_2O_2 + H^{\bullet} \rightarrow H_2O + OH^{\bullet} \quad (3)$$

$$H_2O_2 + H^{\bullet} \rightarrow HO_2 + H_2 \quad (4)$$

$$H_2 + OH^{\bullet} \rightarrow H_2O + H^{\bullet} \quad (5)$$

$$CO + OH^{\bullet} \leftrightharpoons HOCO^{+} \rightarrow H + CO_2 \quad (6)$$

$$\downarrow$$

$$HOCO$$

However, the DRIFTS results show that even slight vacuum conditions (experiments #4 and #5) can lead to a similar intensity of the hydroxyl bands to that which was observed for experiments with $H_2O_2$.

The medium width peak at 1630-1680 $cm^{-1}$ represents ketonic functionality (C=O stretch) This peak is slightly lower in the case of experiments #2 compared to #3, #4, and #5 which means either in the presence of $H_2O_2$ or vacuum pressure more polar functionalities were formed. On the other hand, peaks around 1475-1430 $cm^{-1}$ are related to the formation of aliphatic groups ($-CH_3$ and $-CH_2-$). Figure 7 and 8 suggests almost identical amounts of aliphatic groups are produced in the case of experiments under slight vacuum pressure (experiments #4 and #5). However, in the case of near atmospheric pressure experiments (experiments #2 and #3), more aliphatic chain forms in the presence of $H_2O_2$ (experiment #3) than its

absence (experiment #2). The C≡C stretch bands at 2260-2100 $cm^{-1}$ shows the unsaturated functional groups in the coating film. As Figure 7 and 8 shows, the amounts of unsaturated C≡C functionality is greater in the case of experiments #2 and #3 (near atmospheric pressure) compared to the experiments #4 and #5 (slight vacuum pressure). Thus, it is possible to deduce that longer aliphatic chains with more ketone (C=O stretch) and unsaturated alkyne groups (C≡C stretch) are produced in the presence of $H_2O_2$ and at atmospheric pressure (experiment #3), while at near atmospheric pressure more aliphatic groups are formed. Unsaturated coatings have the possibility of undergoing further reactions to add more functionality to the coating, if desired. On the other hand, slight vacuum pressure can lead to results comparable to $H_2O_2$ injection, at least in terms of the presence of hydroxyl groups. The process economics remain to be analyzed to compare the cost of peroxide to the cost of maintaining a slight vacuum at an industrial scale.

In the case of experiment #6, all observed peaks are of lower intensity. This is attributed to the fact that the acetone solvent was not as efficient in extracting functionalized nanoparticles, given its lower polarity. In fact, qualitative inspection during TEM indicated that fewer nanoparticles were extracted.

## 4. Conclusion

Industrial waste is becoming a real challenge for today's world. Worldwatch Institute projects that the amounts of MSW in the word will increase from today's 1.3 billion tons per year to 2.6 billion tons by 2025 due to urbanization and growing prosperity [46]. On the other hand, the high demand for the production of nanomaterials is estimated to lead to a global market value of $3.3 trillion by 2018 [47]. Conservative market estimates that only for metal oxide nanoparticles, consumption are expected to rise from 270,041 tons in 2012 to 1,663,168 tons by 2020 [48]. In this work we applied PICVD process to investigate the effectiveness of this technique for direct extraction and functional encapsulation of nanoparticles from MSW fly ash powder. Syngas was used as a precursor for polymeric film deposition in the presence of UVC lamps. In some of the experiments, $H_2O_2$ was injected to accelerate photochemical reactions. TEM/EDS results indicate extraction of functionalized nanoparticles thus demonstrating the performance of PICVD. DRIFTS analysis demonstrated formation of polymeric coating with –OH, $–CH_2$, $–CH_3$, C–O, C=O, and C≡C. Moreover, results showed more unsaturated polymeric film forms at atmospheric pressure compared to the vacuum.

Given the massive scale production of ash and syngas as by-products of several processes, the practical implementation of these two materials for extraction of precious materials like coated functionalized

nanoparticles may have a profound impact in several industries such as waste water treatment and construction materials. Subsequent research will focus on treating ash in a fluidized bed reactor, in order to apply higher quantity of ash samples from different sources (coal, cane, oil shale and MSW) under PICVD treatment.

**Acknowledgments**

The authors gratefully acknowledge funding support from the Fonds de recherche du Québec en nature et technologies (FRQNT), the Natural Sciences and Engineering Research Council of Canada (NSERC), as well as École Polytechnique de Montréal. The authors would like to thank the support of centre for Characterization and Microscopy of Materials École Polytechnique de Montréal as well as Mr. Ranjan Roy from the Chemical Engineering Department of McGill University.

**Bibliography**

[1] F. Peng, K. Liang, A. Hu, Nano-crystal glass ceramics obtained from high alumina coal fly ash, Fuel. 84 (2005) 341-346.

[2] S.M. Kulkarni, Kishore, Effects of surface treatments and size of fly ash particles on the compressive properties of epoxy based particulate composites, J. Mater Sci. 37 (2002) 4321-4326.

[3] R.W. Styron, Fly ash composition for use in concrete mix, Google Patents, 2003.

[4] F.H. Gustin, H.P. Shannonhouse, R.W. Styron, Fixation and utilization of ash residue from the incineration of municipal solid waste, Google Patents, 1994.

[5] G. M. Gao, H. F. Zou, S. C. Gan, Z. J. Liu, B. C. An, J. J. Xu, G. H. Li, Preparation and properties of silica nanoparticles from oil shale ash, J. Powder Technol. 191 (2009) 47-51.

[6] N.R.C. Fernandes Machado, D.M. Malachini Miotto, Synthesis of Na–A and –X zeolites from oil shale ash, Fuel. 84 (2005) 2289-2294.

[7] S.N. Azizi, S. Ghasemi, H. Yazdani-Sheldarrei, Synthesis of mesoporous silica (SBA-16) nanoparticles using silica extracted from stem cane ash and its application in electrocatalytic oxidation of methanol, Int. J. Hydrogen Energy. 38 (2013) 12774-12785.

[8] R. Shawabkeh, A. Al-Harahsheh, M. Hami, A. Khlaifat, Conversion of oil shale ash into zeolite for cadmium and lead removal from wastewater, Fuel. 83 (2004) 981-985.

[9] M.L. Oliveira, F. Marostega, S.R. Taffarel, B.K. Saikia, F.B. Waanders, K. DaBoit, B.P. Baruah, L.F. Silva, Nano-mineralogical investigation of coal and fly ashes from coal-based captive power plant (India): an introduction of occupational health hazards, J. Sci. Total Environ. 468-469 (2014) 1128-1137.

[10] L.F. Silva, T. Moreno, X. Querol, An introductory TEM study of Fe-nanominerals within coal fly ash, J. Sci. Total Environ. 407 (2009) 4972-4974.

[11] S. Sadasivan, D.H. Rasmussen, F.P. Chen, R.K. Kannabiran, Preparation and characterization of ultrafine silica, J. Colloids Surf., A: Physicochemical and Engineering Aspects. 132 (1998) 45-52.

[12] N. Mahmood, M.S. Khan, A.U. Khan, K.W. Stöckelhuber, G. Heinrich, Purification, surface modification of coal ash silica and its potential application in rubber composites, J. Appl. Polym. Sci. 117 (2010) 1493-1501.

[13] N. Sombatsompop, S. Thongsang, T. Markpin, E. Wimolmala, Fly ash particles and precipitated silica as fillers in rubbers. I. Untreated fillers in natural rubber and styrene-butadiene rubber compounds, J. Appl. Polym. Sci. 93 (2004) 2119-2130.

[14] A. D'Anna, Combustion-formed nanoparticles, J. P Combust Inst. 32 (2009) 593-613.

[15] H. Cheng, Y. Hu, Municipal solid waste (MSW) as a renewable source of energy: current and future practices in China, Bioresour. Technol. 101 (2010) 3816-3824.

[16] C.C. Wiles, Municipal solid waste combustion ash: State-of-the-knowledge, J. Hazard. Mater. 47 (1996) 325-344.

[17] H.-Y. Wu, Y.-P. Ting, Metal extraction from municipal solid waste (MSW) incinerator fly ash—Chemical leaching and fungal bioleaching, Enzyme Microb. Technol. 38 (2006) 839-847.

[18] F.S. Zhang, H. Itoh, Extraction of metals from municipal solid waste incinerator fly ash by hydrothermal process, J. Hazard. Mater. 136 (2006) 663-670.

[19] K. BeruBe, D. Balharry, K. Sexton, L. Koshy, T. Jones, Combustion-derived nanoparticles: mechanisms of pulmonary toxicity, Clin. Exp. Pharmacol. Physiol. 34 (2007) 1044-1050.

[20] K. Donaldson, L. Tran, L.A. Jimenez, R. Duffin, D.E. Newby, N. Mills, W. MacNee, V. Stone, Combustion-derived nanoparticles: a review of their toxicology following inhalation exposure, Part. Fibre. Toxicol. 2 (2005) 10.

[21] R.D. Hooton, J.A. Bickley, Prescriptive versus performance approaches for durability design – The end of innocence?, Mater. Corro. 63 (2012) 1097-1101.

[22] B. Lothenbach, K. Scrivener, R.D. Hooton, Supplementary cementitious materials, Cem. Concr. Res. 41 (2011) 1244-1256.

[23] A.M. Ramezanianpour, R.D. Hooton, A study on hydration, compressive strength, and porosity of Portland-limestone cement mixes containing SCMs, Cement. Concrete. Comp. 51 (2014) 1-13.

[24] M.D.A. Thomas, R.D. Hooton, A. Scott, H. Zibara, The effect of supplementary cementitious materials on chloride binding in hardened cement paste, , Cem. Concr. Res. 42 (2012) 1-7.

[25] A. Ansarifar, A. Azhar, N. Ibrahim, S.F. Shiah, J.M.D. Lawton, The use of a silanised silica filler to reinforce and crosslink natural rubber, Int. J. Adhes. Adhes. 25 (2005) 77-86.

[26] T. Sabbas, A. Polettini, R. Pomi, T. Astrup, O. Hjelmar, P. Mostbauer, G. Cappai, G. Magel, S. Salhofer, C. Speiser, S. Heuss-Assbichler, R. Klein, P. Lechner, Management of municipal solid waste incineration residues, Waste Manage. 23 (2003) 61-88.

[27] T. Van Gerven, H. Cooreman, K. Imbrechts, K. Hindrix, C. Vandecasteele, Extraction of heavy metals from municipal solid waste incinerator (MSWI) bottom ash with organic solutions, J. Hazard. Mater. 140 (2007) 376-381.

[28] N. Chen, C. Wan, Y. Zhang, Y. Zhang, Effect of nano-$CaCO_3$ on mechanical properties of PVC and PVC/Blendex blend, Polym. Test. 23 (2004) 169-174.

[29] Z. Guo, X. Liang, T. Pereira, R. Scaffaro, H. Thomas Hahn, CuO nanoparticle filled vinyl-ester resin nanocomposites: Fabrication, characterization and property analysis, Compos. Sci. Technol. 67 (2007) 2036-2044.

[30] X.L. Xie, Q.X. Liu, R.K. Y. Li, X.P. Zhou, Q.X. Zhang, Z.Z. Yu, Y.W. Mai, Rheological and mechanical properties of PVC/$CaCO_3$ nanocomposites prepared by in situ polymerization, Polymer. 45 (2004) 6665-6673.

[31] J. Buongiorno, D.C. Venerus, N. Prabhat, T. McKrell, J. Townsend, R. Christianson, Y.V. Tolmachev, P. Keblinski, L.-w. Hu, J.L. Alvarado, I.C. Bang, S.W. Bishnoi, M. Bonetti, F. Botz, A. Cecere, Y. Chang, G. Chen, H. Chen, S.J. Chung, M.K. Chyu, S.K. Das, R. Di Paola, Y. Ding, F. Dubois, G. Dzido, J. Eapen, W. Escher, D. Funfschilling, Q. Galand, J. Gao, P.E. Gharagozloo, K.E. Goodson, J.G. Gutierrez, H. Hong, M. Horton, K.S. Hwang, C.S. Iorio, S.P. Jang, A.B. Jarzebski, Y. Jiang, L. Jin, S. Kabelac, A. Kamath, M.A. Kedzierski, L.G. Kieng, C. Kim, J.H. Kim, S. Kim, S.H. Lee, K.C. Leong, I. Manna, B. Michel, R. Ni, H.E. Patel, J. Philip, D. Poulikakos, C. Reynaud, R. Savino, P.K. Singh, P. Song, T. Sundararajan, E. Timofeeva, T. Tritcak, A.N. Turanov, S. Van Vaerenbergh, D. Wen, S. Witharana, C. Yang, W.H. Yeh, X.Z. Zhao, S.Q. Zhou, A benchmark study on the thermal conductivity of nanofluids, J. Appl. Phys. 106 (2009) 094312.

[32] R. Taylor, S. Coulombe, T. Otanicar, P. Phelan, A. Gunawan, W. Lv, G. Rosengarten, R. Prasher, H. Tyagi, Small particles, big impacts: A review of the diverse applications of nanofluids, J. Appl. Phys. 113 (2013) 011301.

[33] L.S. Sundar, M.H. Farooky, S.N. Sarada, M.K. Singh, Experimental thermal conductivity of ethylene glycol and water mixture based low volume concentration of $Al_2O_3$ and CuO nanofluids, Int Commun Heat Mass Transfer. 41 (2013) 41-46.

[34] S.Y. Fu, X.Q. Feng, B. Lauke, Y.W. Mai, Effects of particle size, particle/matrix interface adhesion and particle loading on mechanical properties of particulate–polymer composites, Compos. Part B-Eng. 39 (2008) 933-961.

[35] R. Hashemi-Nasab, S.M. Mirabedini, Effect of silica nanoparticles surface treatment on in situ polymerization of styrene–butyl acrylate latex, Prog. Org. Coat. 76 (2013) 1016-1023.

[36] C.A. Dorval Dion, J.R. Tavares, Photo-initiated chemical vapor deposition as a scalable particle functionalization technology (a practical review), Powder Technol. 239 (2013) 484-491.

[37] C.A. Dorval Dion, W. Raphael, E. Tong, J.R. Tavares, Photo-initiated chemical vapor deposition of thin films using syngas for the functionalization of surfaces at room temperature and near-atmospheric pressure, Surf. Coat. Technol. 244 (2014) 98-108.

[38] T.A. Egerton, H. Purnama, Does hydrogen peroxide really accelerate $TiO_2$ UV-C photocatalyzed decolouration of azo-dyes such as Reactive Orange 16? Dyes Pigm. 101 (2014) 280-285.

[39] S. Gyergyek, M. Huskić, D. Makovec, M. Drofenik, Superparamagnetic nanocomposites of iron oxide in a polymethyl methacrylate matrix synthesized by in situ polymerization, J. Colloids Surf., A: Physicochemical and Engineering Aspects. 317 (2008) 49-55.

[40] M. Montazer, M. Maali Amiri, ZnO nano reactor on textiles and polymers: ex situ and in situ synthesis, application, and characterization, J. Phys. Chem. B. 118 (2014) 1453-1470.

[41] Z. Guo, T.Y. Kim, K. Lei, T. Pereira, J.G. Sugar, H.T. Hahn, Strengthening and thermal stabilization of polyurethane nanocomposites with silicon carbide nanoparticles by a surface-initiated-polymerization approach, Compos. Sci. Technol. 68 (2008) 164-170.

[42] Y.M. Cao, J. Sun, D.H. Yu, Preparation and properties of nano-$Al_2O_3$ particles/polyester/epoxy resin ternary composites, J. Appl. Polym. Sci. 83 (2002) 70-77.

[43] P.C. Sadek, The HPLC solvent guide, John Wiley, New York: 1996.

[44] K.L. Feilberg, S.R. Sellev, C.J. Nielsen, D.W.T. Griffith, M.S. Johnson, $CO+OH \rightarrow CO_2+H$: The relative reaction rate of five CO isotopologues, J. PCCP. 4 (2002) 4687-4693.

[45] M.J. Frost, P. Sharkey, I.W.M. Smith, Reaction between hydroxyl (deuteroxyl) radicals and carbon monoxide at temperatures down to 80 K: experiment and theory, J. Phys. Chem. 97 (1993) 12254-12259.

[46] W.E. Wilson, A Critical Review of the Gas-Phase Reaction Kinetics of the Hydroxyl Radical, J. Phys. Chem. Ref. Data. 1 (1972) 535-573.

[47] http://www.worldwatch.org/global-municipal-solid-waste-continues-grow (2014).

[48] http://www.prnewswire.com/news-releases/global-market-for-nanotechnology-to-reach-33-trillion-by-2018-181915881 (2014).

[49] http://www.researchandmarkets.com/reports/2488811/the_global_market_for_metal_oxide_nanoparticles (2014).

428 # Figures:

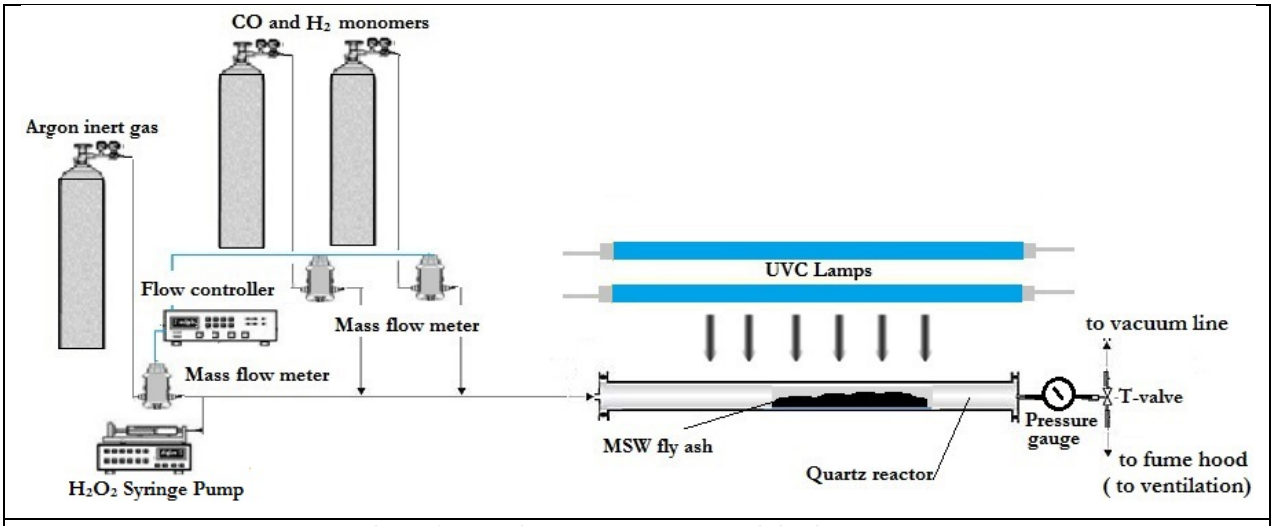


Figure 1. Experimental apparatus and injection set-up

429

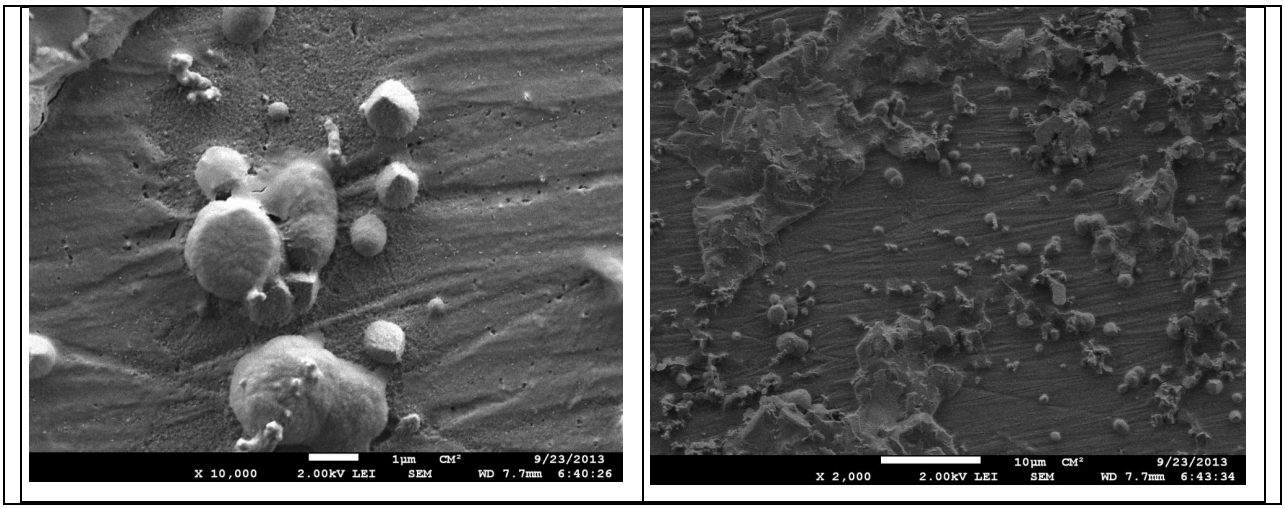

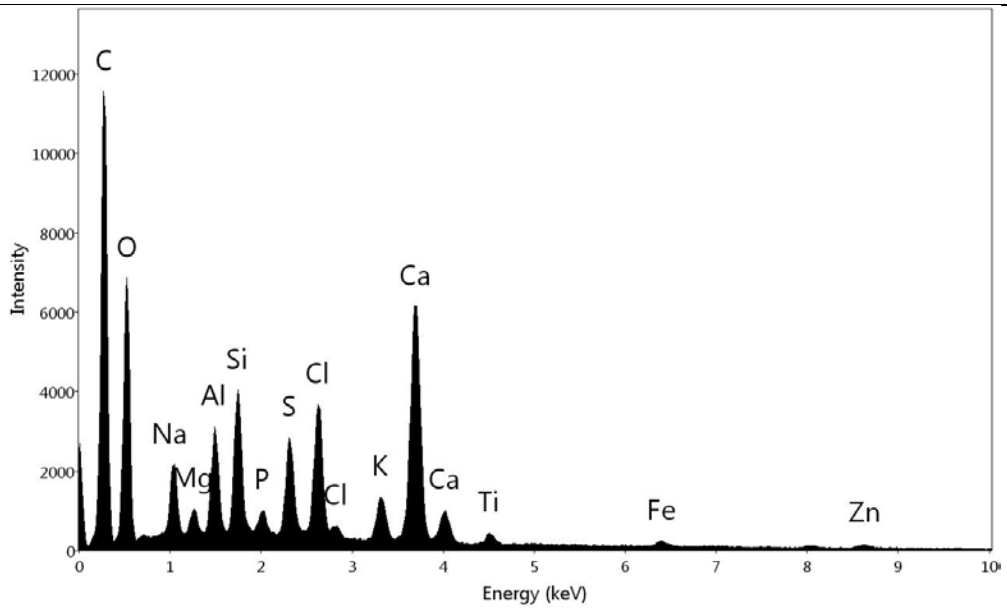


**Figure 2. SEM and EDS micrographs of untreated ash powder**

430

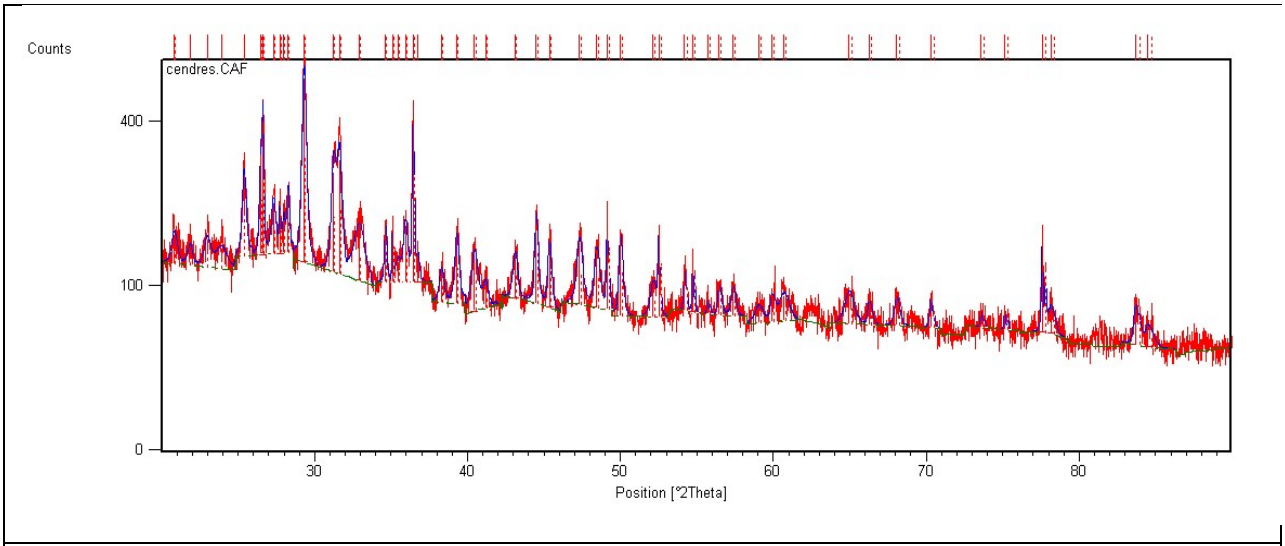


**Figure 3. XRD pattern of ash powder before any experiments.**

431

432

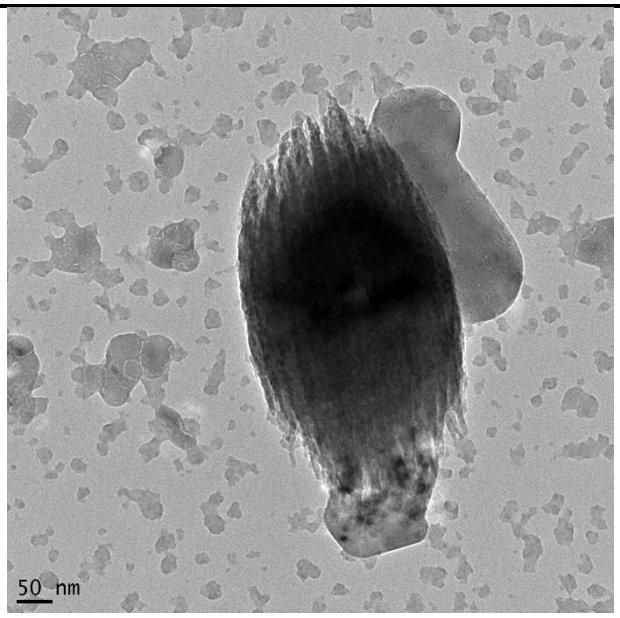


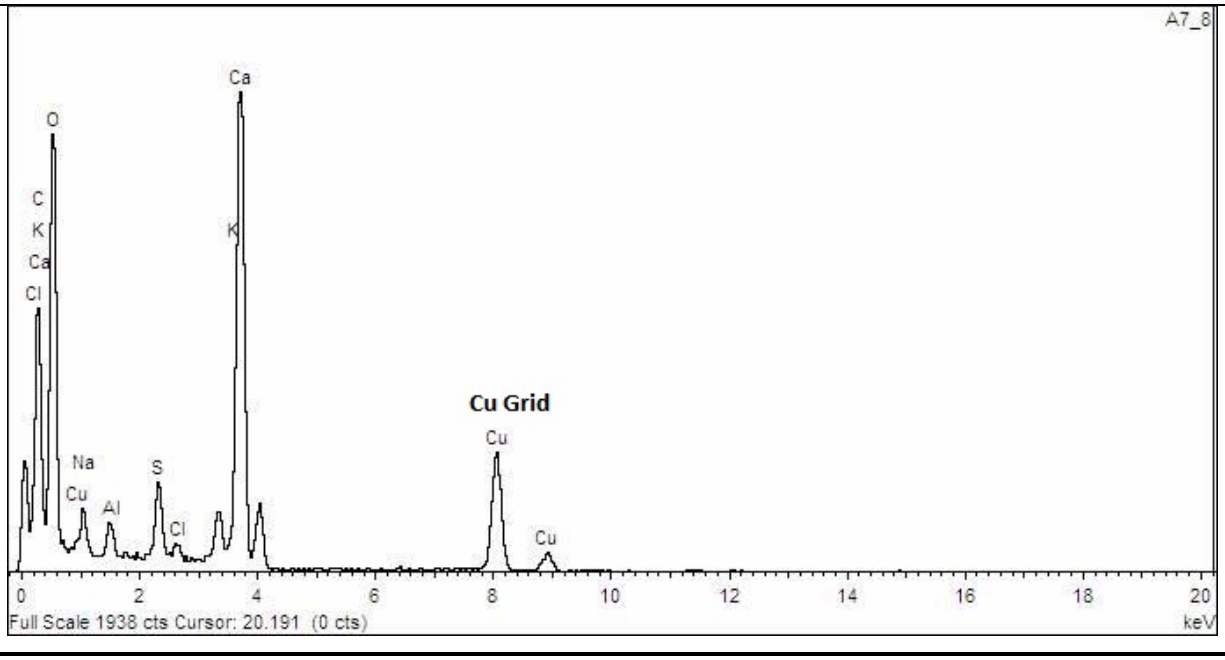


**Figure 4. (a) A single particle identified on a TEM grid from control experiments: Experiment #1 ; (b) The corresponding EDS spectrum shows its composition is mainly Ca.**

433

| (a) | (b) |
|---|---|

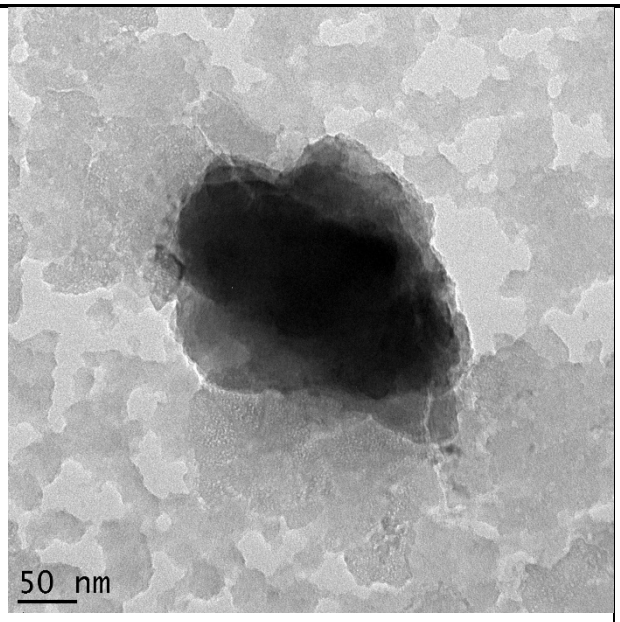


(c)

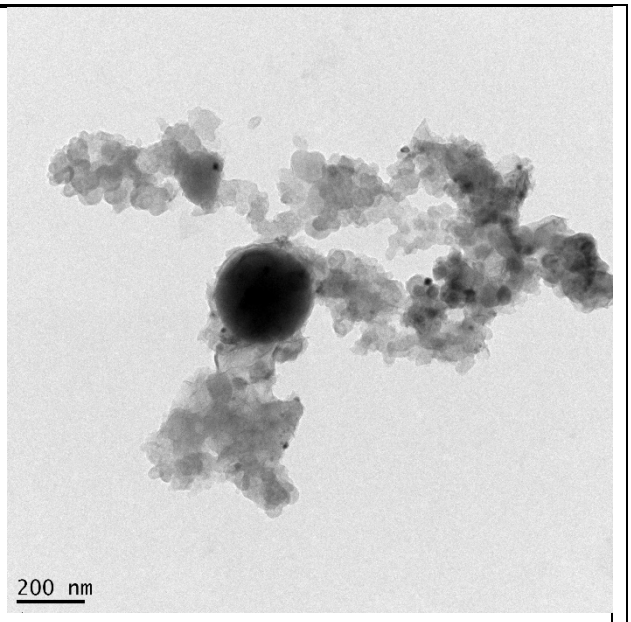


(d)

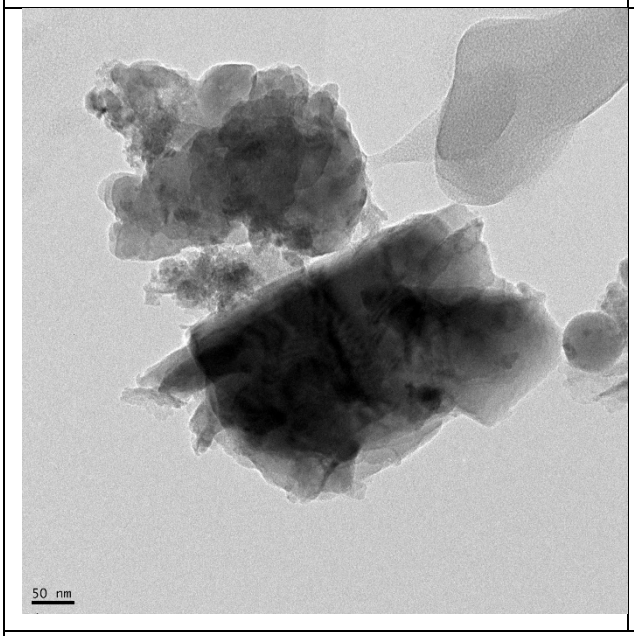


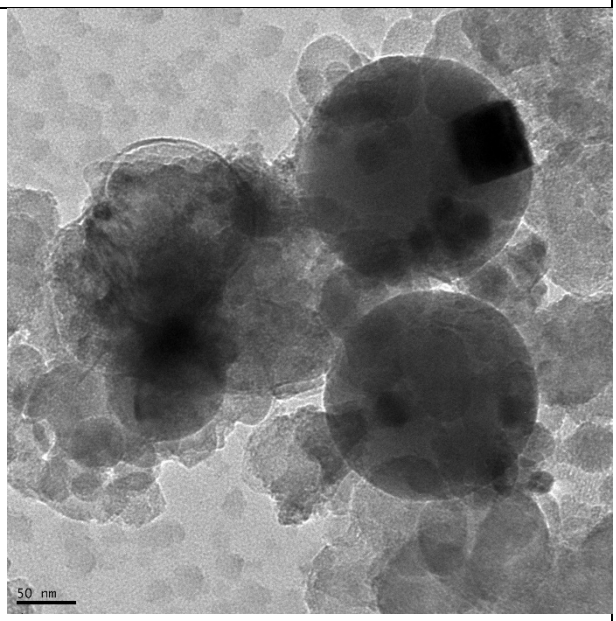


(e)

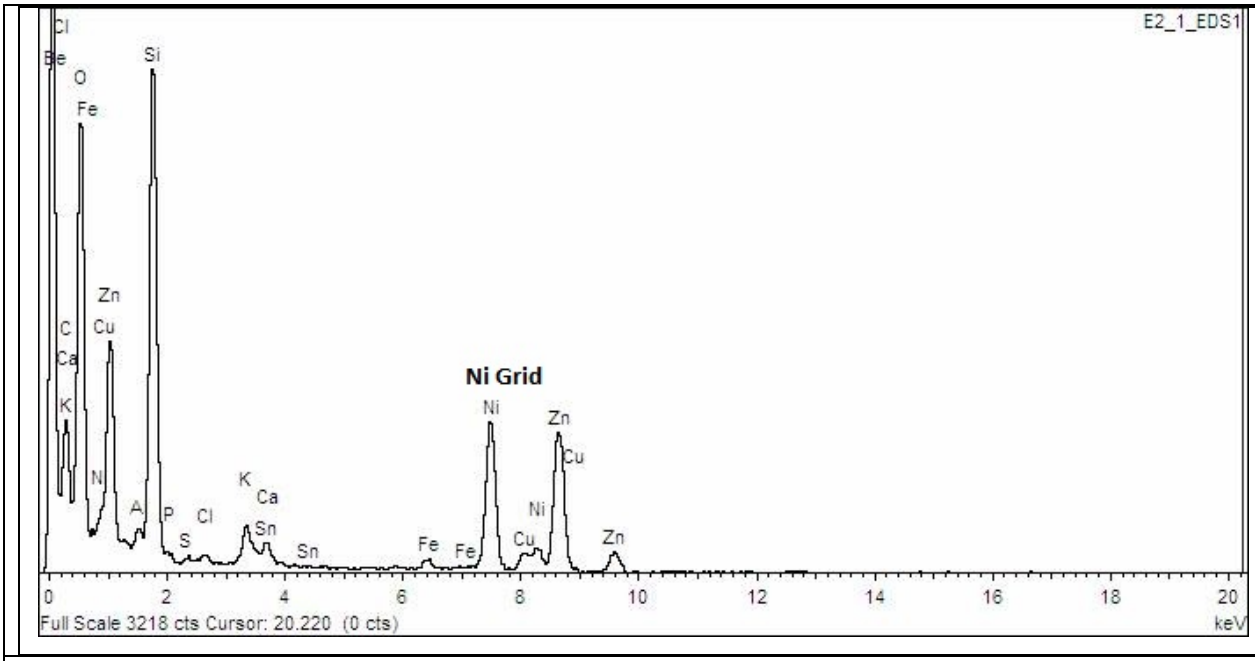


**Figure 5. TEM micrographs of treated samples (a) Experiment #2, (b) Experiment #3, (c) Experiment #4, (d) Experiment #5, (e) Representative of EDS spectrum taken from experiment #3**

434

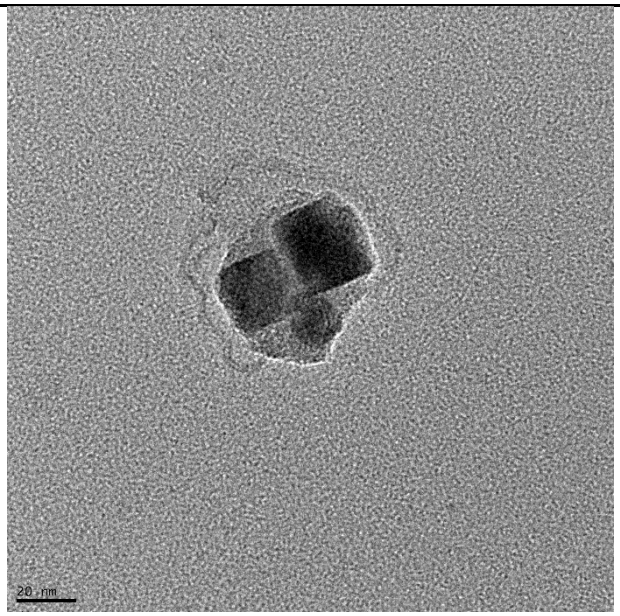

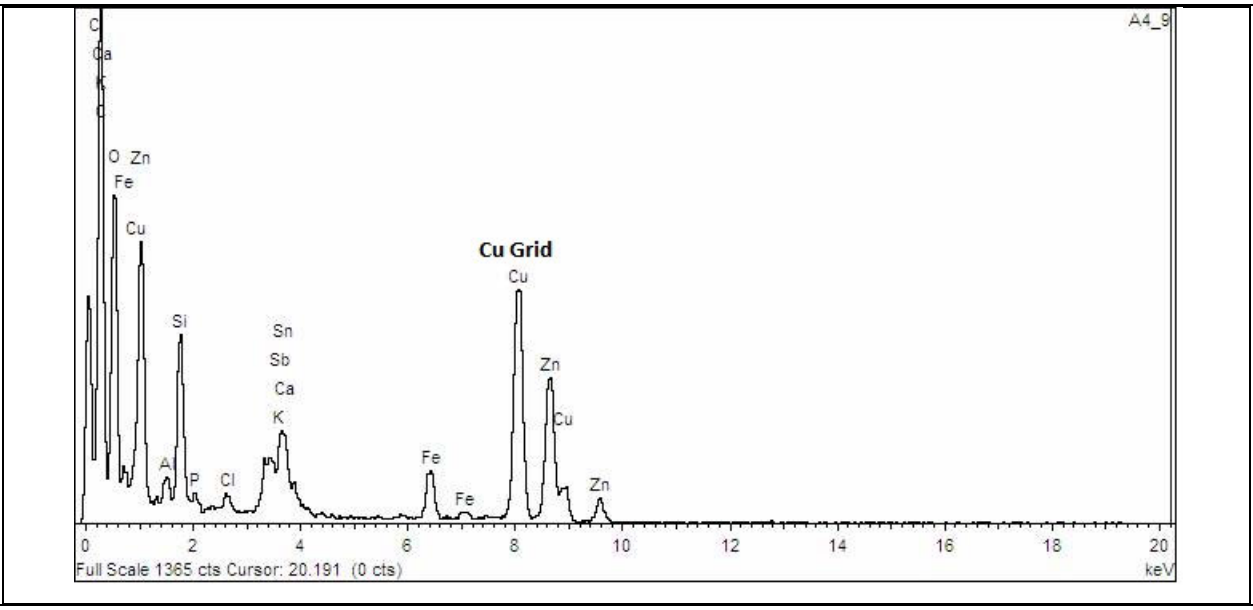


**Figure 6. TEM micrographs of treated samples (a) Experiment #6, (b) Representative of EDS spectrum.**

435

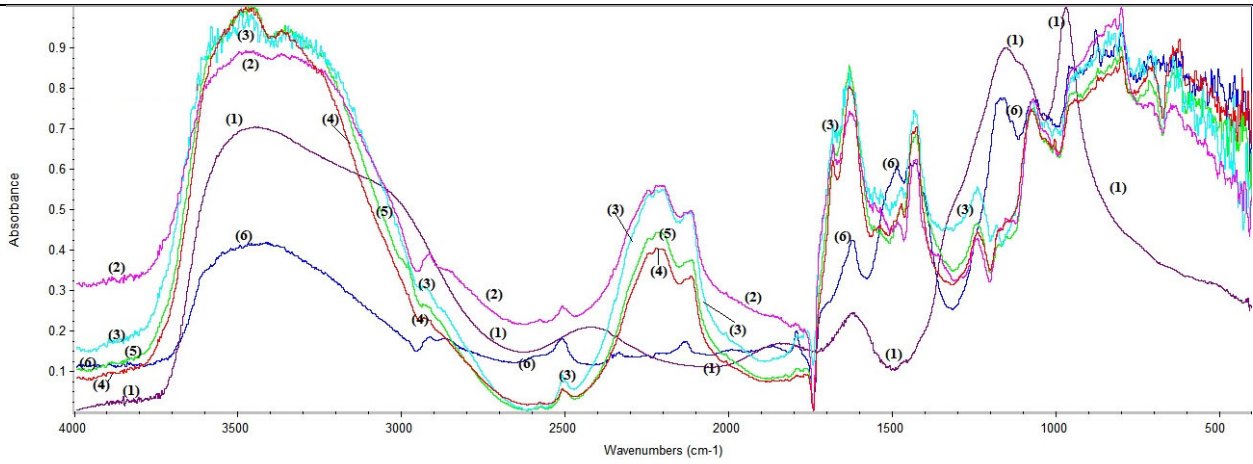


**Figure 7. DRIFTS spectra comparison for PICVD process: (1) Experiment #1, (2) Experiment #2, (3) Experiment #3, (4) Experiment #4, (5) Experiment #5, (6) Experiment #6.**

436

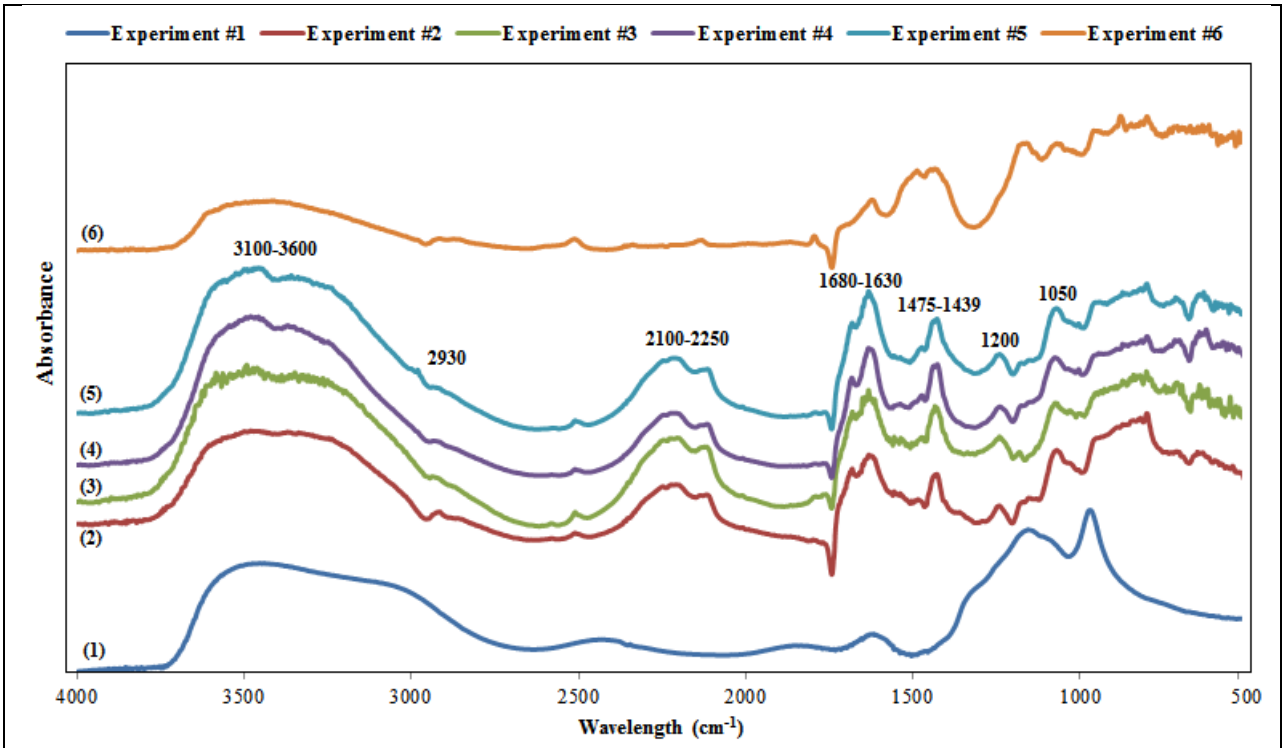


Figure 8. DRIFTS spectra for PICVD process along with peaks identifications: (1) Experiment #1, (2) Experiment #2, (3) Experiment #3, (4) Experiment #4, (5) Experiment #5, (6) Experiment #6.

## Tables:

Table 1. Experimental details

| Experiment Number | $H_2O_2$ injection | UVC Lamps | Dispersion medium | Pressure |
|---|---|---|---|---|
| #1 | No | Off | Water | Near atmospheric (+10 kPa) |
| #2 | No | On | Water | Near atmospheric (+10 kPa) |
| #3 | Yes | On | Water | Near atmospheric (+10 kPa) |
| #4 | No | On | Water | Slight vacuum (-10 kPa) |
| #5 | Yes | On | Water | Slight vacuum (-10 kPa) |
| #6 | No | On | Acetone | Near atmospheric (+10 kPa) |

**Table 2. Elemental concentration of ash powder using ICP-AES analysis**

| **Element** | **Ag** | **Al** | **As** | **B** | **Be** |
|---|---|---|---|---|---|
| **Wavelength** | 328.06 | 396.15 | 189.04 | 249.77 | 313.04 |
| **Concentration (ppm)** | 0.26 | 37.41 | 1.09 | 0.21 | 0.00 |
| **Std Dev:** | 0.00 | 0.19 | 0.00 | 0.00 | 0.00 |
| **Equivalent oxide basis (%wt)** [1] | 0.01% | 2.58% | 0.06% | 0.02% | 0.00% |
| **Element** | **Ca** | **Cd** | **Co** | **Cr** | **Cu** |
| **Wavelength** | 393.30 | 214.43 | 228.61 | 206.55 | 221.81 |
| **Concentration (ppm)** | 1495.55 | 1.59 | 0.20 | 1.70 | 8.45 |
| **Std Dev:** | 0.15 | 0.00 | 0.00 | 0.00 | 0.01 |
| **Equivalent oxide basis (%wt)** [1] | 76.37% | 0.07% | 0.01% | 0.09% | 0.39% |
| **Element** | **Fe** | **K** | **Mg** | **Mn** | **Mo** |
| **Wavelength** | 259.94 | 766.49 | 279.55 | 257.61 | 202.03 |
| **Concentration (ppm)** | 191.63 | 7.27 | 84.51 | 9.41 | 0.21 |
| **Std Dev:** | 0.01 | 0.04 | 0.77 | 0.06 | 0.00 |
| **Equivalent oxide basis (%wt)** [1] | 10.00% | 0.32% | 5.11% | 0.54% | 0.01% |
| **Element** | **Na** | **Ni** | **Pb** | **Sb** | **Se** |
| **Wavelength** | 589.59 | 231.60 | 220.35 | 217.58 | 196.09 |
| **Concentration (ppm)** | 7.66 | 1.11 | 19.71 | 11.52 | 0.11 |
| **Std Dev:** | 0.03 | 0.00 | 0.01 | 0.03 | 0.00 |
| **Equivalent oxide basis (%wt)** [1] | 0.38% | 0.05% | 0.83% | 0.56% | 0.01% |
| **Element** | **Si** | **Ti** | **Tl** | **V** | **Zn** |
| **Wavelength** | 251.61 | 334.94 | 351.92 | 292.40 | 213.85 |
| **Concentration (ppm)** | 0.07 | 6.24 | 0.00 | 0.45 | 48.00 |
| **Std Dev:** | 0.00 | 0.03 | 0.08 | 0.00 | 0.14 |
| **Equivalent oxide basis (%wt)** [1] | 0.01% | 0.38% | 0.00% | 0.03% | 2.18% |

[1]Equivalant oxide basis was calculated based on the higher oxidation form e.g. $Fe_2O_3$ instead of FeO.

442

**Table 3. Peak assignment in the infrared spectra of dried samples under PICVD coating process**

| **Peak absorption band ($cm^{-1}$)** | **Peak assignment** |
|---|---|
| 3600-3100 | Hydroxyl group, hydrogen-bonded, O-H stretch in aliphatic alcohol |
| 1350-1260 | Primary or secondary alcohol, O-H in plane bend |
| ~ 1050 | Primary alcohol, C-O stretch |
| ~ 1200 | Phenol, C-O stretch |
| 3000-2800 | Asymmetric and symmetric methyl ($-CH_3$) and methylene ($-CH_2-$) stretch |
| 2250-2100 | C ≡ C stretch in alkynes |
| 1680-1630 | C=O stretch in ketones |
| 1475-1430 | $-CH_3$ asymmetric and $-CH_3$ asymmetric methyl bending in aliphatic compounds |

443